# A Further Look at $Q_1$ and $Q_2$ from TOGA COARE

Richard H. Johnson, * Paul E. Ciesielski

*Colorado State University, Fort Collins, Colorado*

Thomas M. Rickenbach

*Department of Geography, East Carolina University, Greenville, North Carolina*

* *Corresponding author address:* Richard H. Johnson, Department of Atmospheric Science, Colorado State University, Fort Collins CO 80523.

E-mail: johnson@atmos.colostate.edu

## ABSTRACT

Two features of Yanai et al.'s profiles of $Q_1$ and $Q_2$ – the commonly observed double-peak structure to $Q_2$ and an inflection in the $Q_1$ profile below the melting level – are explored using estimates of convective and stratiform rainfall partitioning based on Massachusetts Institute of Technology (MIT) radar reflectivity data collected during TOGA COARE. The MIT radar data allow the $Q_1$ and $Q_2$ profiles to be classified according to stratiform rain fraction within the radar domain and, within the limitations of the data sets, interpretations to be made about the relative contributions of convective and stratiform precipitation to the mean profiles.

The sorting of $Q_2$ by stratiform rain fraction leads to the confirmation of previous findings that the double-peak structure in the mean profile is a result of a combination of separate contributions of convective and stratiform precipitation. The convective contribution gives a lower drying peak, which when combined with the stratiform component drying peak aloft (along with moistening at low levels), yields the double-peak structure. With respect to the inflection in the $Q_1$ profile below 600 hPa or 4 km, this feature appears to be a manifestation of cooling by melting just below the 0°C level, which has a prominent impact due to the broad areal coverage of stratiform precipitation. We conclude, then, that the rather subtle features in the $Q_1/Q_2$ profiles of Yanai et al. are directly linked to effects of stratiform precipitation systems, which are integral components of tropical convection.

# 1. Introduction

A conceptual breakthrough in understanding how tropical cloud systems interact with their environment was achieved through the landmark paper of Yanai et al. (1973), wherein the now-familiar $Q_1$ (apparent heat source) and $Q_2$ (apparent moisture sink) were defined. However, well prior to the 1973 study, Yanai (1961) introduced $Q_1$ and $Q_2$ in a paper entitled "A Detailed Analysis of Typhoon Formation," which investigated the dynamic and thermodynamic properties of the formation of typhoon Doris 1958 in the western Pacific. Vertical profiles of $Q_1$ and $Q_2$ – the first ever to be presented– were shown in Yanai (1961) for the period of the transformation of Doris from a cold-core to warm-core tropical cyclone.

Following Yanai et al. (1973), but including ice processes, we write the equations for the apparent heat source and moisture sink as follows:

$$\begin{aligned} Q_1 &\equiv \frac{\partial \bar{s}}{\partial t} + \bar{\mathbf{v}} \cdot \nabla \bar{s} + \bar{\omega} \frac{\partial \bar{s}}{\partial p} \\ &= L_v(\bar{c} - \bar{e}) + (L_v + L_f)(\bar{d} - \bar{s}_*) + L_f(\bar{f} - \bar{m}) + Q_R - \frac{\partial}{\partial p}(\overline{s'\omega'}) \ , \end{aligned} \tag{1}$$

$$\begin{aligned} Q_2 &\equiv -L_v \left[ \frac{\partial \bar{q}}{\partial t} + \bar{\mathbf{v}} \cdot \nabla \bar{q} + \bar{\omega} \frac{\partial \bar{q}}{\partial p} \right] \\ &= L_v(\bar{c} - \bar{e}) + L_v(\bar{d} - \bar{s}_*) + L_v \frac{\partial}{\partial p}(\overline{q'\omega'}) \ , \end{aligned} \tag{2}$$

where $c$, $e$, $d$, $s_*$, $f$, and $m$ are condensation, evaporation, deposition, sublimation, freezing, and melting rates; $q$ is the water vapor mixing ratio; $s \equiv c_p T + gz$ the dry static energy; $Q_1$ the apparent heat source; $Q_2$ the apparent moisture sink; $Q_R$ the net radiative heating rate; $L_v$ and $L_f$ the latent heats of vaporization and fusion; overbar refers to a horizontal average; and primes a deviation from this average.

Yanai et al. (1973) used 1956 Marshall Islands sounding data to compute $Q_1$ and $Q_2$ and then applied a simplified cloud model to diagnose the bulk properties of cumulus ensembles, which provided substantial insight into properties of tropical convective systems and how

they impact their environment. The profiles of $Q_1$ and $Q_2$ obtained by Yanai et al. (1973) for the Marshall Islands for the period 15 April–22 July 1956 are shown in Fig. 1, along with radiative heating $Q_R$ estimates from Dopplick (1972). They found a primary peak in $Q_1$ in the upper troposphere, whereas the principal $Q_2$ peak was in the lower troposphere. Yanai et al. (1973) pointed out that the separation of the $Q_1$ and $Q_2$ peaks is indicative of vigorous deep convection, i.e., strong vertical eddy fluxes of moist static energy $h(\equiv s+L_v q)$. Since the profiles are averages over a three-month period, they represent contributions from both convective and stratiform components of precipitation systems, which have distinctly different heating and moistening profiles (Houze 1982, 1989; Johnson 1984). Just how the structure of the heating profile varies in the vertical is of considerable interest, since that determines the dynamical response of the environment to convection (Hartmann et al. 1984; Raymond and Jiang 1990; Nicholls et al. 1991; Schumacher et al. 2004).

A curious feature of the $Q_2$ profile is its double-peaked structure, which has also been found for the GARP Atlantic Tropical Experiment (GATE) (Esbensen et al. 1988), as well as for other experiments such as the more recent *Mirai* Indian Ocean Cruise for the Study of the MJO Onset (MISMO) (Katsumata et al. 2011). This feature has been attributed by Johnson (1984) and Esbensen et al. (1988) to the separate contributions of convective and stratiform precipitation systems. Namely, condensation and deposition aloft associated with stratiform precipitation produces the upper peak while condensation in convective precipitation the lower peak. Placed in a time perspective, the vertical motion and hence heating and drying typically undergo an evolution (on time scales ranging from diurnal to the life cycle of tropical cloud clusters) from a low-level peak in the vertical motion (and heating) in the early stages to an upper-level peak in the later stages Houze (1982); Johnson and Young (1983). This evolution has since been documented on longer time scales ranging up to the 30-60 day Madden-Julian Oscillation (MJO), as reviewed by Kiladis et al. (2009).

It is the purpose of this article to delve further into the relationship between the $Q_1$ and $Q_2$ profiles and convective/stratiform rain partitioning using radar and sounding data

from an experiment which is now celebrating its twentieth anniversary – the 1992-93 Tropical Ocean Global Atmosphere Coupled Ocean-Atmosphere Response Experiment (TOGA COARE) conducted in the western Pacific (Webster and Lukas 1992). However, we first note that the experiment-mean TOGA COARE $Q_1$ and $Q_2$ profiles (Johnson and Ciesielski 2000) are different from those of the Marshall Islands, GATE, and MISMO. To illustrate this difference, a comparison of the mean profiles for MISMO and TOGA COARE is shown in Fig. 2 (from Katsumata et al. 2011). Notably absent from the COARE results are low-level peaks in heating and drying. This behavior was also found over the northern South China Sea during the May-June 1998 South China Sea Monsoon Experiment (SCSMEX; Johnson and Ciesielski 2002). Johnson and Lin (1987) explained the unique feature of the COARE profiles as a consequence of frequent trade-wind-like, nonprecipitating cumulus clouds during the quiescent and westerly-wind-burst phases of the MJO. These clouds were prevalent during dry midtropospheric conditions and served to moisten the lower troposphere, thereby producing prolonged periods of negative $Q_2$, as also observed during the Barbados Oceanographic and Meteorological Experiment (BOMEX; Nitta and Esbensen 1974). In contrast, during the active phase of the MJO, $Q_1$ and $Q_2$ distributions much like those of Yanai et al. (1973) were observed (Fig. 3 of Johnson and Lin 1987).

In this paper we will use radar data from the Massachusetts Institute of Technology (MIT) radar aboard the *R/V Vickers* during COARE (Rickenbach and Rutledge 1998) to relate the heating and moistening profiles to the stratiform/convective rain fractions derived by that radar to further elucidate the factors contributing to the observed mean $Q_1$ and $Q_2$ profiles for that experiment.

# 2. Data and analysis procedures

*a. Radar data*

Radar reflectivity data from the MIT C-band Doppler radar, deployed aboard the *R/V Vickers* processed by Rickenbach and Rutledge (1998) are used in this study. The position of the *Vickers* within the COARE Intensive Flux Array (IFA) is shown in Fig. 3 along with other sounding sites in the region used in the budget analyses. (Rickenbach and Rutledge 1998, their Fig. 2) indicate the time periods of the radar and sounding operations during the four-month COARE Intensive Observing Period (IOP: November 1992–February 1993). Convective/stratiform rain partitioning was carried out using a slight modification of the method of Steiner et al. (1995) applied to 10-min radar reflectivity volumes. The mean stratiform rain fraction for the three cruises of the *Vickers* was determined to be 28%, somewhat less than the ∼40% estimate for this region by Schumacher and Houze (2003) obtained from the Tropical Rainfall Measuring Mission (TRMM) precipitation radar (PR). However, as we will see later, the MIT-based estimate is somewhat greater if we remove the periods of trade wind cumulus from the average.

*b. Sounding data and averaging methodology*

Six-hourly sounding data were objectively analyzed onto a 1° by 1° grid at 25-hPa intervals from 1000 to 25 hPa over the large-scale COARE domain using procedures described in Ciesielski et al. (1997) and incorporating humidity sensor corrections as outlined in Ciesielski et al. (2003). The resulting gridded basic and derived fields were then averaged over the circular MIT radar coverage area shown in Fig. 3. The distribution of sounding sites in proximity to the *Vickers* is reasonably good, so analyses over this region are deemed fairly reliable, apart from other issues such as data gaps and random sampling errors (Mapes et al. 2003).

# 3. Results for four-month TOGA COARE Intensive Observing Period

A time series of $Q_1$ and $Q_2$ for the COARE IOP is shown in Fig. 4, along with the stratiform rainfall fraction based on MIT radar data for the three cruises of the *Vickers* and average rainfall for the MIT radar coverage area derived from the moisture budget, where the Woods Hole Oceanographic Institution IMET (Improved METeorology) buoy is used for surface evaporation. A prominent MJO event occurred in December, characterized by a transition from shallow convection (low-level peak in $Q_2$) early in the month followed by deep convection mid-month and then stratiform precipitation (drying above moistening) at the end of the month (Lin and Johnson 1996). Consistent with this evolution is an increasing trend in the stratiform rainfall fraction through December as determined by the MIT radar.

Conspicuous in Fig. 4 are several ∼10-day to two-week periods of negative $Q_2$ in the lower troposphere. These features were described by Johnson and Lin (1987) as episodes of trade-wind-like shallow cumulus existing during very dry low-to-midtroposphere conditions. The moistening in November occurred during light surface wind conditions, whereas the episodes in late-December and February were during strong winds. They noted that when winds were strong during these shallow cumulus periods, there was greater moistening (negative $Q_2$) near cloud base in association with sub-inversion (Esbensen 1978) or forced (Stull 1985) type cumuli that were, in part, a manifestation of overshooting boundary layer eddies. When winds were light, the cumuli were slightly deeper ["inversion penetrating" after Esbensen (1978) or "active" after Stull (1985)] and the moistening peaked in the upper part of the cloud layer (similar to the Atlantic trades, Nitta and Esbensen 1974). Higher sea-surface temperature (by 1 K) and weaker shear observed during the November period likely contributed to the more active cumuli at that time.

# 4. Relating $Q_1$ and $Q_2$ to stratiform rain fraction

The frequent occurrence of trade-wind regimes over the warm pool during COARE can be attributed to "dry intrusions" that were observed in association with the MJO (Parsons and Coauthors 1994; Numaguti et al. 1995; Yoneyama and Fujitani 1995; Mapes and Zuidema 1996), which helped to inhibit the growth of convection (e.g., Redelsperger et al. 2002). Johnson and Lin (1987) focused on $Q_1$ and $Q_2$ during these trade-wind-like periods by averaging the profiles for times when precipitation was less than 3.5 mm day$^{-1}$, the average surface evaporation rate during COARE. Alternatively, to explore the characteristics of deep convection during COARE, we *remove* the effects of these periods by including only those times when the precipitation *exceeded* 3.5 mm day$^{-1}$. The resulting $Q_1/Q_2$ profiles are shown in Fig. 5. They now look much like those of Yanai et al. (1973) in Fig. 1, namely, possessing a double-peak structure to $Q_2$ (though with several additional peaks) and an inflection in the $Q_1$ profile near 650 hPa.[1] Therefore, to interpret the Yanai et al. (1973) profiles in light of the COARE results, we subsequently restrict analyses to the dates and times that make up Fig. 5 (a total of 184 six-hour periods).

$Q_1$ and $Q_2$ profiles as a function of stratiform rain fraction (SRF) are shown in Fig. 6. As SRF increases, there is a transition from vertically separated, single peaks in heating and drying in the low- to midtroposphere to nearly coincident peaks at higher levels, consistent with an evolution in the precipitation from mostly convective to mainly stratiform in character (Luo and Yanai 1984). The evolution for $Q_2$ is more complex than that for $Q_1$, with multiple drying peaks aloft above a moistening peak in the lower troposphere. The low-level drying peaks between 700 and 800 hPa for SRF>40% likely reflect the effects of convection coexisting with stratiform precipitation.

[1]Both the Marshall Islands and the western Pacific $Q_1$ profiles also show peaks near 150 hPa. These peaks may not represent any physical processes, rather they may be artifacts of applying the boundary condition $\omega = 0$ at the tropopause or 100 hPa such that some upward motion acting on weak stability above the lapse-rate minimum (Fueglistaler et al. 2009) produces a local heating maximum.

Another way of viewing this transition is by comparing profiles for different values of SRF (Fig. 7). In this plot SRF values shown are averages for the following SRF bins: <20%, 20-30%, 30-40%, 40-50%, 50-60%, and >60%. The number of cases in each bin is 41, 53, 29, 17, 15, and 29, respectively. Although there is considerable noise in the profiles (especially for $Q_2$), the transition from convective to stratiform structure with increasing SRF can clearly be seen. Also evident for large values of SRF is an inflection in the $Q_1$ profile below 600 hPa near 4 km. This feature has been attributed to cooling by melting, which has been seen in observations (e.g., Johnson et al. 1996) and cloud-resolving models (e.g., Shie et al. 2003). The inflection in $Q_1$ is also observed in the Yanai et al. (1973) Marshall Islands $Q_1$ profile (Fig. 1).

Due to the abundant precipitation over the warm pool, melting leaves a measurable and persistent effect on the static stability. Melting takes place over a relatively shallow layer (∼300-400 m deep, Willis and Heymsfield 1989) below the 0°C level. Freezing of hydrometeors occurs at levels above 0°C, but over a deeper layer; nevertheless, the combined effects of freezing above melting serves to increase the static stability at the 0°C level and also from $L_v(\bar{f} - \bar{m})$ in (1), the vertical gradient in $Q_1$ there. However, when computing $Q_1$ from sounding data, it is the LHS of (1) that is calculated and since the vertical advection term $\bar{\omega}\partial\bar{s}/\partial p$ is usually the dominant term in that calculation, the impact of freezing and melting perturbs $\partial\bar{s}/\partial p$ and hence the $Q_1$ profile. To illustrate this effect, a time series of static stability, represented as $dT/dz$ in Fig. 8, shows a persistent stable layer in proximity to 0°C. This stable layer is strongest during periods of heaviest rainfall, so its linkage to melting is perceptible. Also seen in Fig. 8 is a persistent, though fluctuating in intensity, trade-wind stable layer, which tends to be strongest during periods of light rainfall and negative low-level $Q_2$ (Fig. 4).

Because the stratiform precipitation systems cover large areas, their impact on the temperature field is significant. This effect is seen in Fig. 9, where for SRF > 50%, a shallow cool anomaly is present in a layer below the melting level, accompanied by a deeper moist

layer aloft. For the largest values of SRF, there are both warm and dry anomalies centered just below 800 hPa. These features are manifestations of "onion soundings," often observed in association with the stratiform precipitation regions of tropical squall lines or cloud clusters (Zipser 1977). This structure can also be seen in Fig. 10, a plot of the mean relative humidity for SRF>60% and <20%. For large values of SRF, moist conditions exist above 0°C, indicative of stratiform anvil clouds aloft, with dry conditions below. In contrast, the mostly convective situations (SRF<20%) are characterized by a relatively dry mid- to upper troposphere. The two contrasting profiles in Fig. 10 are consistent with the bimodal relative humidity behavior (drought and rainy periods) reported by Brown and Zhang (1997) for COARE. For the lowest values of SRF (Fig. 9), dry conditions are observed in the midtroposphere, which suppress cloud development.

Also observed for large SRF values (Fig. 9) is a layer of cooling near the tropopause ($\sim$150 hPa), a feature commonly observed atop mesoscale convective systems in the tropics (Johnson and Kreite 1982; Holloway and Neelin 2007). In addition, a cool anomaly is observed near the surface for increasing values of SRF, indicative of extensive modification of the boundary layer by downdrafts as the stratiform rain amounts and associated area coverage increases (Zipser 1977; Fitzjarrald and Garstang 1981).

In the computation of $Q_2$ from large-scale fields, the dominant term is $\bar{\omega}\partial\bar{q}/\partial p$. Time series of the individual contribution to this term are shown in Fig. 11. There is a clear upward shift in the vertical motion peak as SRF increases. The average SRF for the cases considered here (those for rainfall exceeding 3.5 mm day$^{-1}$) is 36%, somewhat higher than the 28% for the entire MIT radar period. Viewing the $\bar{\omega}$ time series and noting that half the rain is above SRF = 36% and half below, it is readily apparent that the double-peak structure to $Q_2$ arises from the individual convective and stratiform contributions.

To confirm that the term involving $\bar{\omega}\partial\bar{q}/\partial p$ is the principal contributor to $Q_2$, time series of both fields are shown in Fig. 12. Overall, the broad pattern and evolution of both fields are similar, showing distinctly different vertical structures for small and large values of SRF.

# 5. Summary and conclusions

It has been four decades since the landmark paper of Yanai et al. (1973) diagnosing apparent heat sources $Q_1$ and moisture sinks $Q_2$, as well as convective transports based on a simplified cloud model, using Marshall Islands data. In subsequent years, numerous field campaigns in the tropics and midlatitudes have been conducted computing $Q_1$ and $Q_2$, with results similar to those of Yanai et al. In this paper we explore aspects of those heating and moistening profiles using estimates of convective and stratiform rainfall partitioning based on MIT radar reflectivity data from the *R/V Vickers* during TOGA COARE (Rickenbach and Rutledge 1998). Particular attention is given to (i) the commonly observed double-peak structure to $Q_2$ and (ii) an inflection in the $Q_1$ profile below the melting level.

The MIT radar data allow the $Q_1$ and $Q_2$ profiles to be classified according to stratiform rain fraction and, within the limitations of the data sets, interpretations to be made about the relative contributions of convective and stratiform precipitation to the mean profiles. Radar data from the three cruises of the *Vickers* are used along with gridded fields constructed from the COARE sounding array and averaged over the MIT radar coverage area. To remove periods when trade-wind-like cumulus were present during COARE, times were selected for analysis when the average rainfall rate over the MIT area exceeded 3.5 mm day$^{-1}$. This criterion resulted in 184 six-hourly periods, for which the average stratiform rain fraction was 36%.

The sorting of $Q_2$ by stratiform rain fraction leads to the conclusion that its double-peak structure is a result of the separate contributions of convective and stratiform precipitation, as suggested by Johnson (1984), Esbensen et al. (1988), and others. The convective contribution gives a lower drying peak, which when combined with the stratiform contribution of a drying peak aloft (along with moistening at low levels), yields the double-peak structure. With respect to the inflection in the $Q_1$ profile below 600 hPa or 4 km, this feature appears to be a manifestation of cooling by melting just below the 0°C level, which has a prominent impact due to the broad areal coverage of stratiform precipitation. We conclude, then, that

the rather subtle features in the $Q_1/Q_2$ profiles of Yanai et al. (1973) are directly linked to effects of stratiform precipitation systems, years ago identified by Zipser (1969, 1977) and Houze (1977) as integral components of tropical convection. With the recent completion of the DYNAMO (Dynamics of the MJO) field campaign in the Indian Ocean (October 2011–March 2012), the opportunity exists to further extend this analysis to another tropical ocean basin.

*Acknowledgments.*

This article is prepared as a tribute to Michio Yanai in honor of his enormous contributions to the field of atmospheric science. The research has been supported by the National Science Foundation, under grants AGS-0966758, AGS-1059899 and AGS-1118141, and the National Aeronautics and Space Administration under grant NNX10AG81G.

# REFERENCES


Brown, R. G. and C. Zhang, 1997: Variability of midtropospheric moisture and its effect on cloud-top height distribution during TOGA COARE. *J. Atmos. Sci.*, **54**, 2760–2774.

Ciesielski, P. E., L. Hartten, and R. H. Johnson, 1997: Impacts of merging profiler and rawinsonde winds on TOGA COARE analyses. *J. Atmos. Oceanic Technol.*, **14**, 1264–1279.

Ciesielski, P. E., R. H. Johnson, P. T. Haertel, and J. Wang, 2003: Corrected TOGA COARE sounding humidity data: Impact on diagnosed properties of convection and climate over the warm pool. *J. Climate*, **16**, 2370–2384.

Dopplick, T. G., 1972: Radiative heating of the global atmosphere. *J. Atmos. Sci.*, **29**, 1278–1294.

Esbensen, S., 1978: Bulk thermodynamic effects and properties of small tropical cumuli. *J. Atmos. Sci.*, **35**, 826–837.

Esbensen, S. K., J.-T. Wang, and E. I. Tollerud, 1988: A composite life cycle of nonsquall mesoscale convective systems over the tropical ocean. part II: Heat and moisture budgets. *J. Atmos. Sci.*, **45**, 537–548.

Fitzjarrald, D. R. and M. Garstang, 1981: Vertical structure of the tropical boundary layer. *Mon. Wea. Rev.*, **109**, 1512–1526.

Fueglistaler, S., A. E. Dessler, T. J. Dunkerton, I. Folkins, Q. Fu, and P. W. Mote, 2009: Tropical tropopause layer. *Rev. Geophys.*, **47**, 1004, doi:10.1029/2008RG000267.

Hartmann, D. L., H. H. Hendon, and R. A. Houze, Jr., 1984: Some implications of the mesoscale circulations in tropical cloud clusters for large-scale dynamics and climate. *J. Atmos. Sci.*, **41**, 113–121.

Holloway, C. E. and J. D. Neelin, 2007: The convective cold top and quasi-equilibrium. *J. Atmos. Sci.*, **64**, 1467–1487.

Houze, R. A., Jr., 1977: Structure and dynamics of a tropical squall-line system. *Mon. Wea. Rev.*, **105**, 1540–1567.

Houze, R. A., Jr., 1982: Cloud clusters and large-scale vertical motion in the tropics. *J. Meteor. Soc. Japan*, **60**, 396–410.

Houze, R. A., Jr., 1989: Observed structure of mesoscale convective systems and implications for large-scale heating. *Quart. J. Roy. Meteor. Soc.*, **115**, 425–461.

Johnson, R. H., 1984: Partitioning tropical heat and moisture budgets into cumulus and mesoscale components: Implications for cumulus parameterization. *Mon. Wea. Rev.*, **112**, 1590–1601.

Johnson, R. H. and P. E. Ciesielski, 2000: Rainfall and radiative heating rate estimates from TOGA COARE atmospheric budgets. *J. Atmos. Sci.*, **57**, 1497–1514.

Johnson, R. H. and P. E. Ciesielski, 2002: Characteristics of the 1998 summer monsoon onset over the northern South China Sea. *J. Meteor. Soc. Japan*, **80**, 561–578.

Johnson, R. H., P. E. Ciesielski, and K. A. Hart, 1996: Tropical inversions near the 0°C level. *J. Atmos. Sci.*, **53**, 1838–1855.

Johnson, R. H. and D. C. Kreite, 1982: Thermodynamic and circulation characteristics of winter monsoon tropical mesoscale convection. *Mon. Wea. Rev.*, **110**, 1898–1911.

Johnson, R. H. and X. Lin, 1987: Episodic trade wind regimes over the western Pacific warm pool. *J. Atmos. Sci.*, **54**, 2020–2034.

Johnson, R. H. and G. S. Young, 1983: Heat and moisture budgets of tropical mesoscale anvil clouds. *J. Atmos. Sci.*, **40**, 2138–2147.

Katsumata, M., P. E. Ciesielski, and R. H. Johnson, 2011: Evaluation of budget analysis during MISMO. *J. Appl. Meteor. Climatol.*, **40**, 241–254.

Kiladis, G. N., M. C. Wheeler, P. T. Haertel, K. H. Straub, and P. E. Roundy, 2009: Convectively coupled equatorial waves. *Rev. Geophys.*, **47**, 2003, doi:10.1029/2008RG000266.

Lin, X. and R. H. Johnson, 1996: Kinematic and thermodynamic characteristics of the flow over the western Pacific warm pool during TOGA COARE. *J. Atmos. Sci.*, **53**, 695–715.

Luo, H. and M. Yanai, 1984: The large-scale circulation and heat sources over the Tibetan Plateau and surrounding areas during the early summer of 1979. part ii: Heat and moisture budgets. *Mon. Wea. Rev.*, **112**, 966–989.

Mapes, B. E., P. E. Ciesieslki, and R. H. Johnson, 2003: Sampling errors in rawinsonde-array budgets. *J. Atmos. Sci.*, **60**, 2697–2714.

Mapes, B. E. and P. Zuidema, 1996: Radiative-dynamical consequences of dry tongues in the tropical troposphere. *J. Atmos. Sci.*, **53**, 620–638.

Nicholls, M. E., R. A. Pielke, and W. R. Cotton, 1991: Thermally forced gravity waves in an atmosphere at rest. *J. Atmos. Sci.*, **48**, 1869–1884.

Nitta, T. and S. Esbensen, 1974: Heat and moisture budget analyses using BOMEX data. *Mon. Wea. Rev.*, **102**, 17–28.

Numaguti, A., R. Oki, K. Nakamura, K. Tsuboki, T. Asai, and Y.-M. Kodama, 1995: 4-5 day-period variations and low-level dry air observed in the equatorial western Pacific during the TOGA-COARE IOP. *J. Meteor. Soc. Japan*, **73**, 267–290.

Parsons, D. and Coauthors, 1994: The integrated sounding system: Description and preliminary observations from TOGA COARE. *Bull. Amer. Meteor. Soc.*, **75**, 553–567.

Raymond, D. J. and H. Jiang, 1990: A theory for long-lived mesoscale convective systems. *J. Atmos. Sci.*, **47**, 3067–3077.

Redelsperger, J.-L., D. Parsons, and F. Guichard, 2002: Recovery processes and factors limiting cloud-top height following the arrival of a dry intrusion observed during TOGA COARE. *J. Atmos. Sci.*, **59**, 2438–2457.

Rickenbach, T. M. and S. A. Rutledge, 1998: Convection in TOGA COARE: Horizontal scale, morphology, and rainfall production. *J. Atmos. Sci.*, **55**, 2715–2729.

Schumacher, C. and R. A. Houze, Jr., 2003: Stratiform rain in the tropics as seen by the TRMM precipitation radar. *J. Climate*, **16**, 1739–1756.

Schumacher, C., R. A. Houze, Jr., and I. Kraucunas, 2004: The tropical dynamical response to latent heating estimates derived from the trmm precipitation radar. *J. Atmos. Sci.*, **61**, 1341–1358.

Shie, C.-L., W.-K. Tao, J. Simpson, and C.-H. Sui, 2003: Quasi-equilibrium states in the tropics simulated by a cloud-resolving model. part i: Specific features and budget analysis. *J. Climate*, **16**, 817–833.

Steiner, M., R. A. Houze, and S. E. Yuter, 1995: Climatological characterization of three-dimensional storm structure from operational radar and rain gauge data. *J. Appl. Meteor. Climatol.*, **34**, 1978–2007.

Stull, R. B., 1985: A fair-weather cumulus cloud classification scheme for mixed-layer studies. *J. Climate Appl. Meteor.*, **24**, 49–56.

Webster, P. J. and R. Lukas, 1992: TOGA COARE: The coupled ocean-atmosphere response experiment. *Bull. Amer. Meteor. Soc.*, **73**, 1377–1416.

Willis, P. T. and A. J. Heymsfield, 1989: Structure of the melting layer in mesoscale convective system stratiform precipitation. *J. Atmos. Sci.*, **46**, 2008–2025.

347 Yanai, M., 1961: A detailed analysis of typhoon formation. *J. Meteor. Soc. Japan*, **39**,
348 187–214.

349 Yanai, M., S. Esbensen, and J.-H. Chu, 1973: Determination of bulk properties of tropical
350 cloud clusters from large-scale heat and moisture budgets. *J. Atmos. Sci.*, **30**, 611–627.

351 Yoneyama, K. and T. Fujitani, 1995: The behavior of dry westerly air associated with con-
352 vection observed during TOGA-COARE R/V Natsushima cruise. *J. Meteor. Soc. Japan*,
353 **73**, 291–304.

354 Zipser, E. J., 1969: The role of organized unsaturated convective downdrafts in the structure
355 and rapid decay of an equatorial disturbance. *J. Appl. Meteor.*, **8**, 799–814.

356 Zipser, E. J., 1977: Mesoscale and convective-scale downdrafts as distinct components of
357 squall-line circulation. *Mon. Wea. Rev.*, **105**, 1568–1589.

# List of Figures

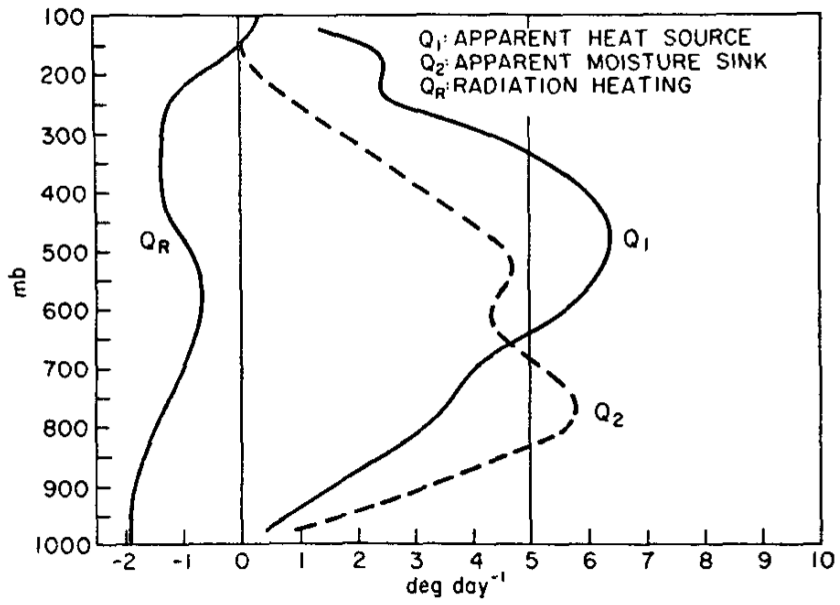


FIG. 1. Apparent heat source $Q_1$, apparent moisture sink $Q_2$, and net radiative heating rate for Marshall Islands. From Yanai et al. (1973).

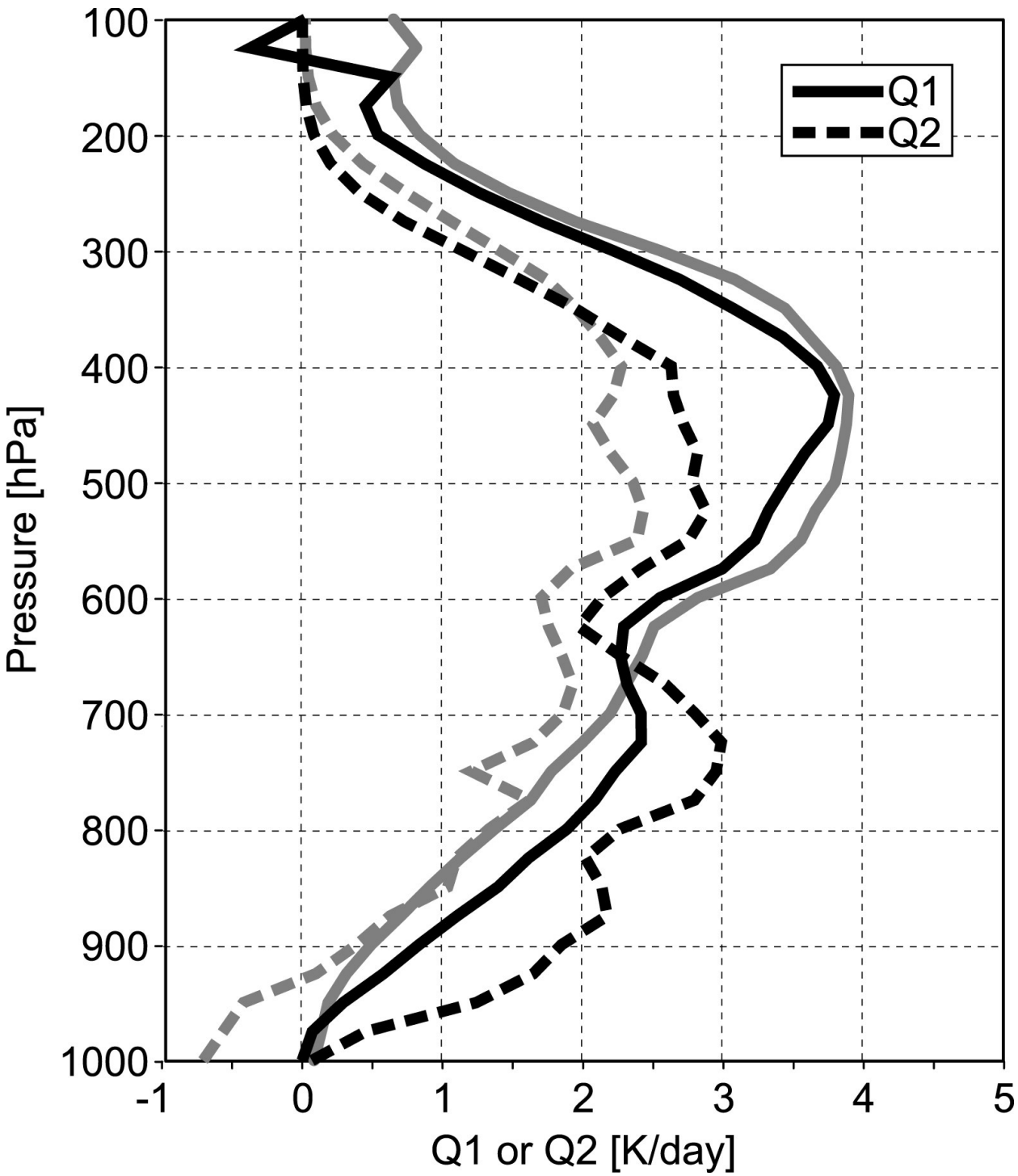


FIG. 2. Apparent heat source $Q_1$ and apparent moisture sink $Q_2$ for MISMO in the Indian Ocean (dark curve) and TOGA COARE IFA (light curve). From Katsumata et al. (2011).

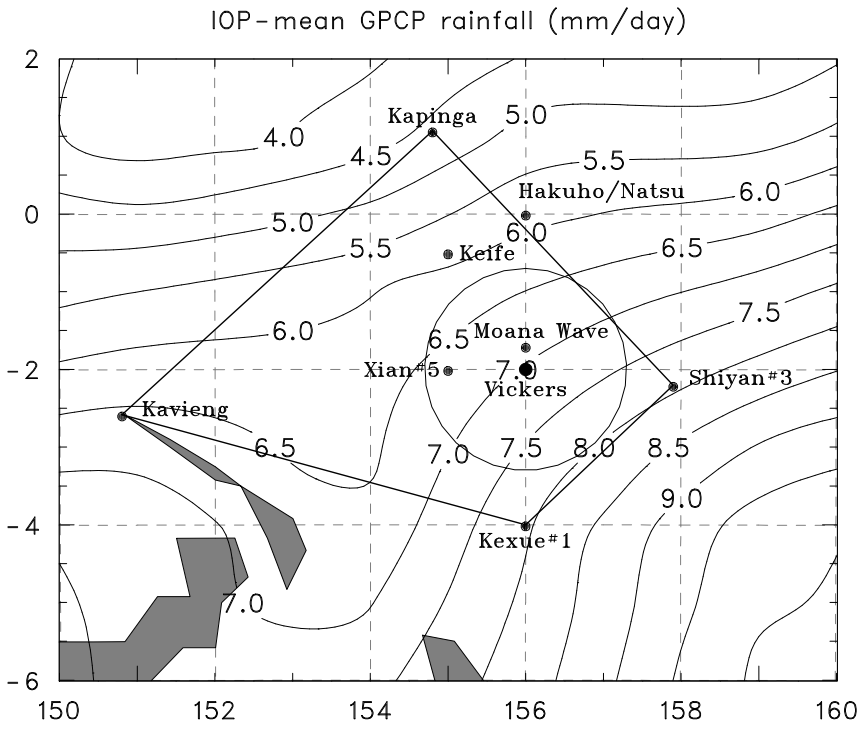


FIG. 3. TOGA COARE Intensive Flux Array (solid lines), atmospheric sounding sites, and 4-month mean COARE rainfall (color; mm day$^{-1}$) from Global Precipitation Climatology Project (GCPC). Circle indicates 120-km radius radar study area. MIT radar was aboard *R/V Vickers*.

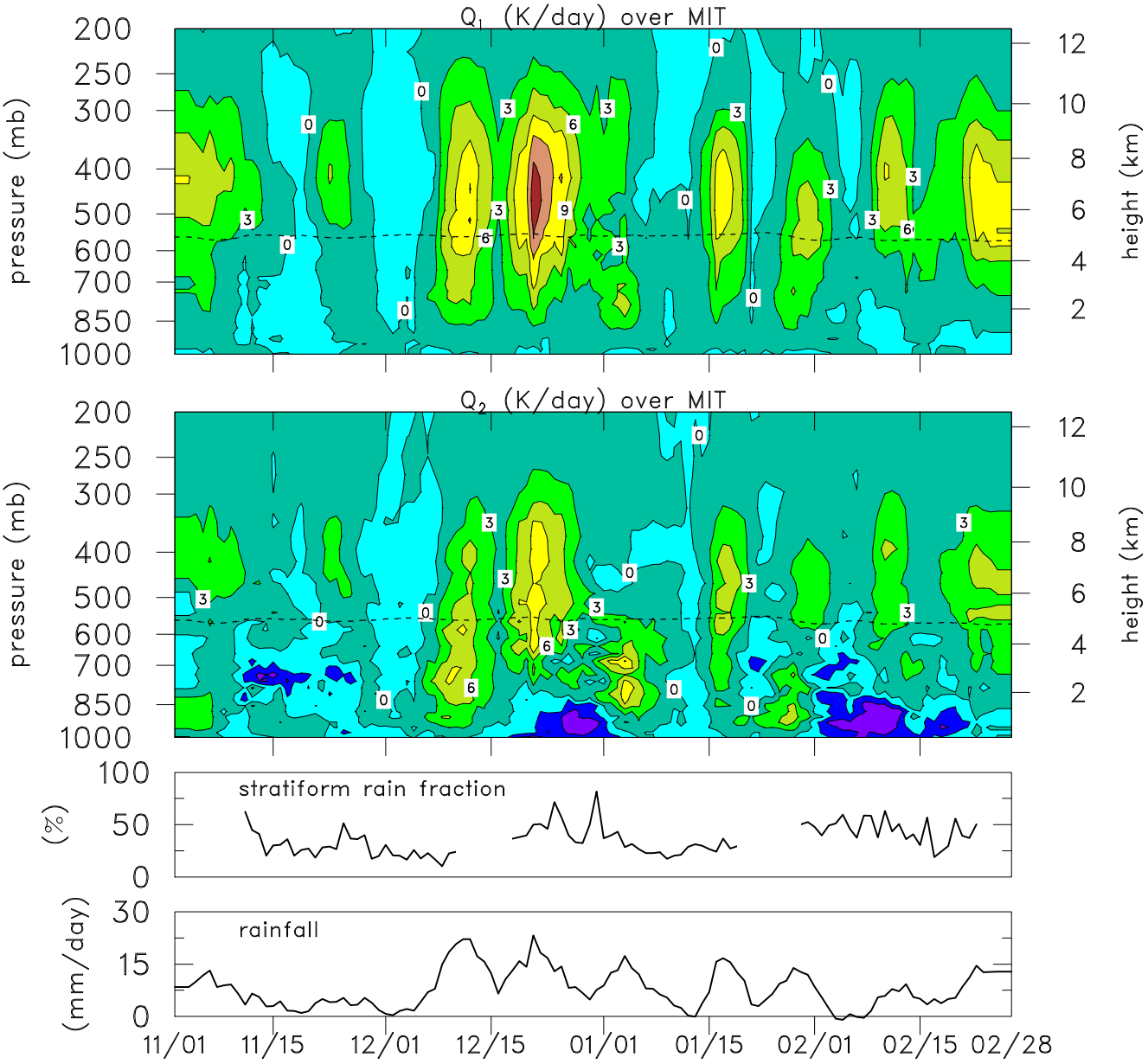


FIG. 4. (top panels) TOGA COARE IOP time series of $Q_1$ and $Q_2$, horizontal line indicates 0° level; (third panel) time series of stratiform rain fraction; and (bottom panel) moisture-budget-derived rainfall. Budget fields and rainfall have been smoothed with a 5-day running mean filter. All fields are for MIT radar area.

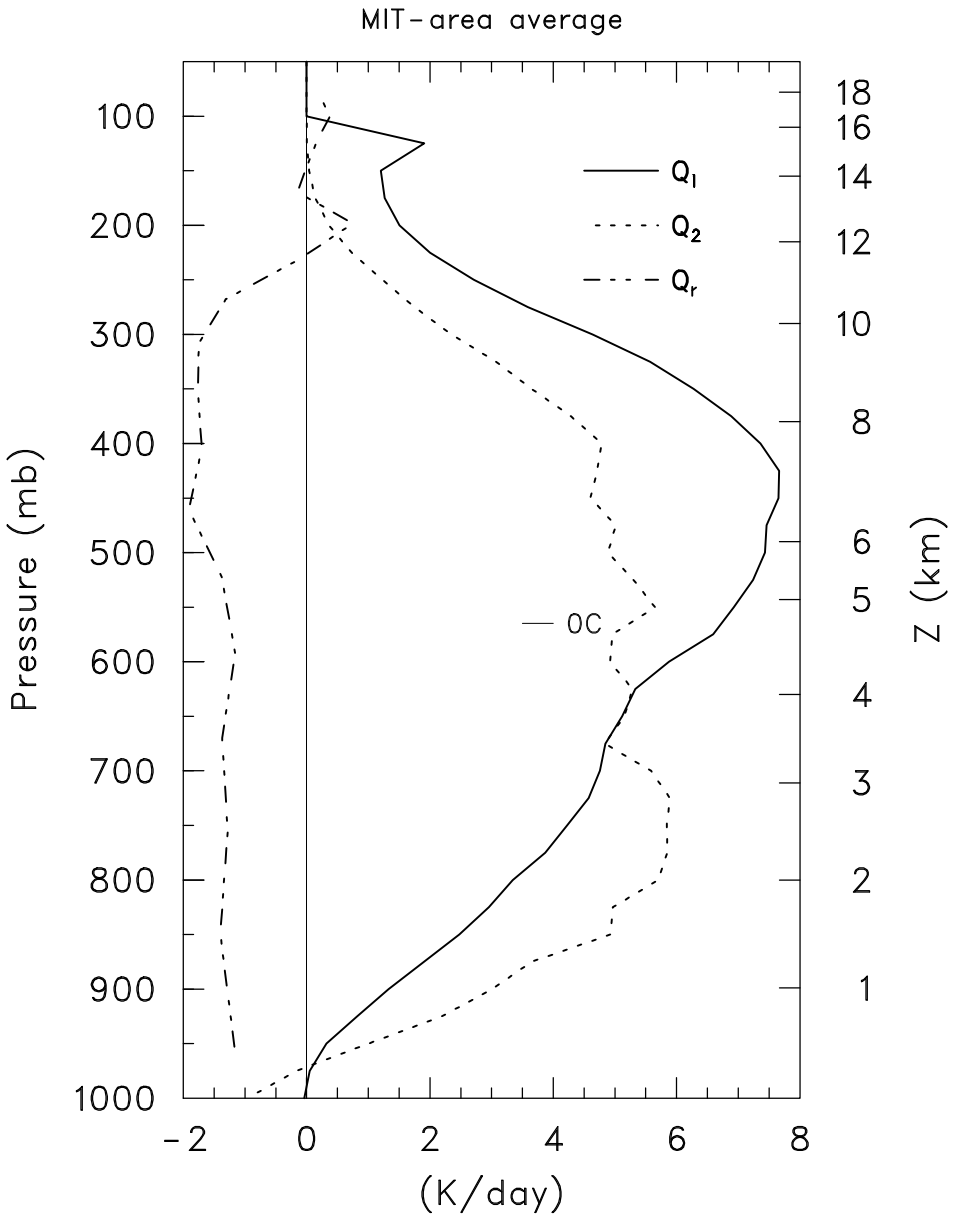


FIG. 5. Average $Q_1$ and $Q_2$ profiles for MIT radar coverage area for times when precipitation from the atmospheric moisture budget over this area exceeded 3.5 mm day$^{-1}$. $Q_R$ profile is from L'Ecuyer and Stephens (2003) based on 13-yr (1998-2011) mean over this region. 0°C level is indicated.

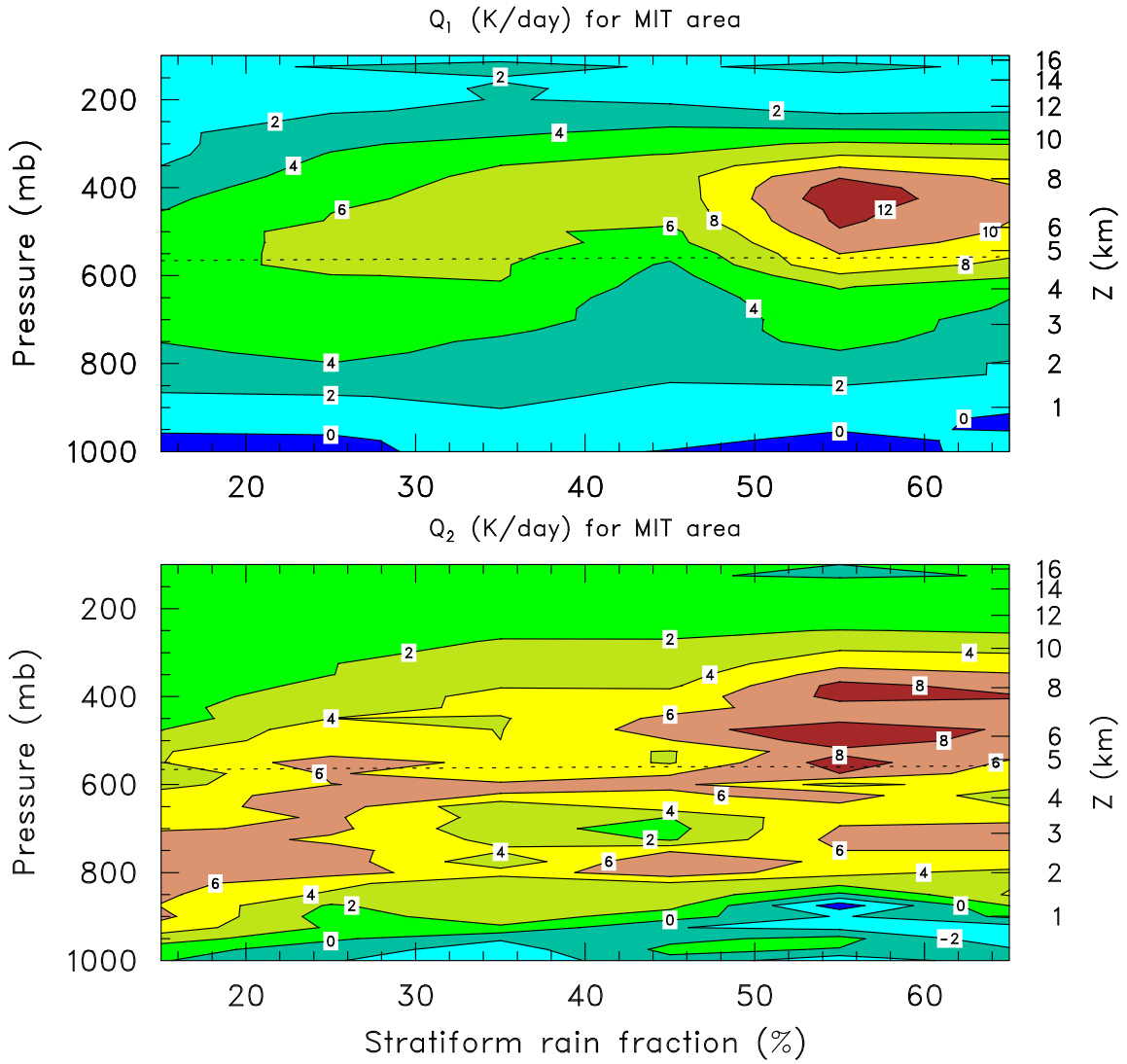


FIG. 6. (top) $Q_1$ and (bottom) $Q_2$ (K day$^{-1}$ as a function of stratiform rain fraction for the MIT radar coverage area during TOGA COARE for times when moisture-budget-derived rainfall over that area exceeded 3.5 mm day$^{-1}$. Dashed line indicates 0°C level.

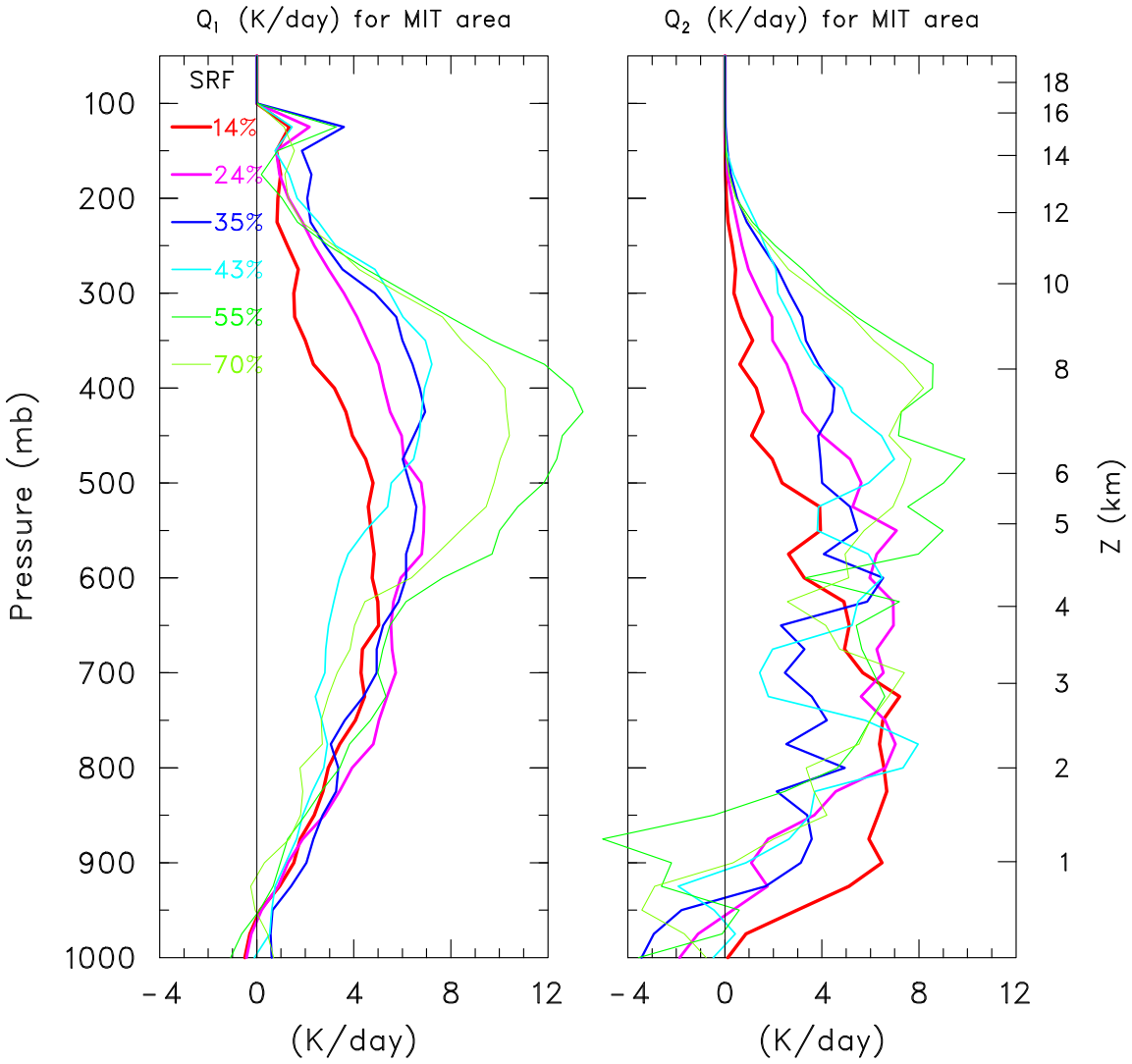


FIG. 7. $Q_1$ and $Q_2$ profiles as a function of stratiform rain fraction for the MIT radar coverage area during TOGA COARE for times when moisture-budget-derived rainfall over that area exceeded 3.5 mm day$^{-1}$. SRF values plotted are averages for the following SF bins: <20%, 20-30%, 30-40%, 40-50%, 50-60%, and >60%.

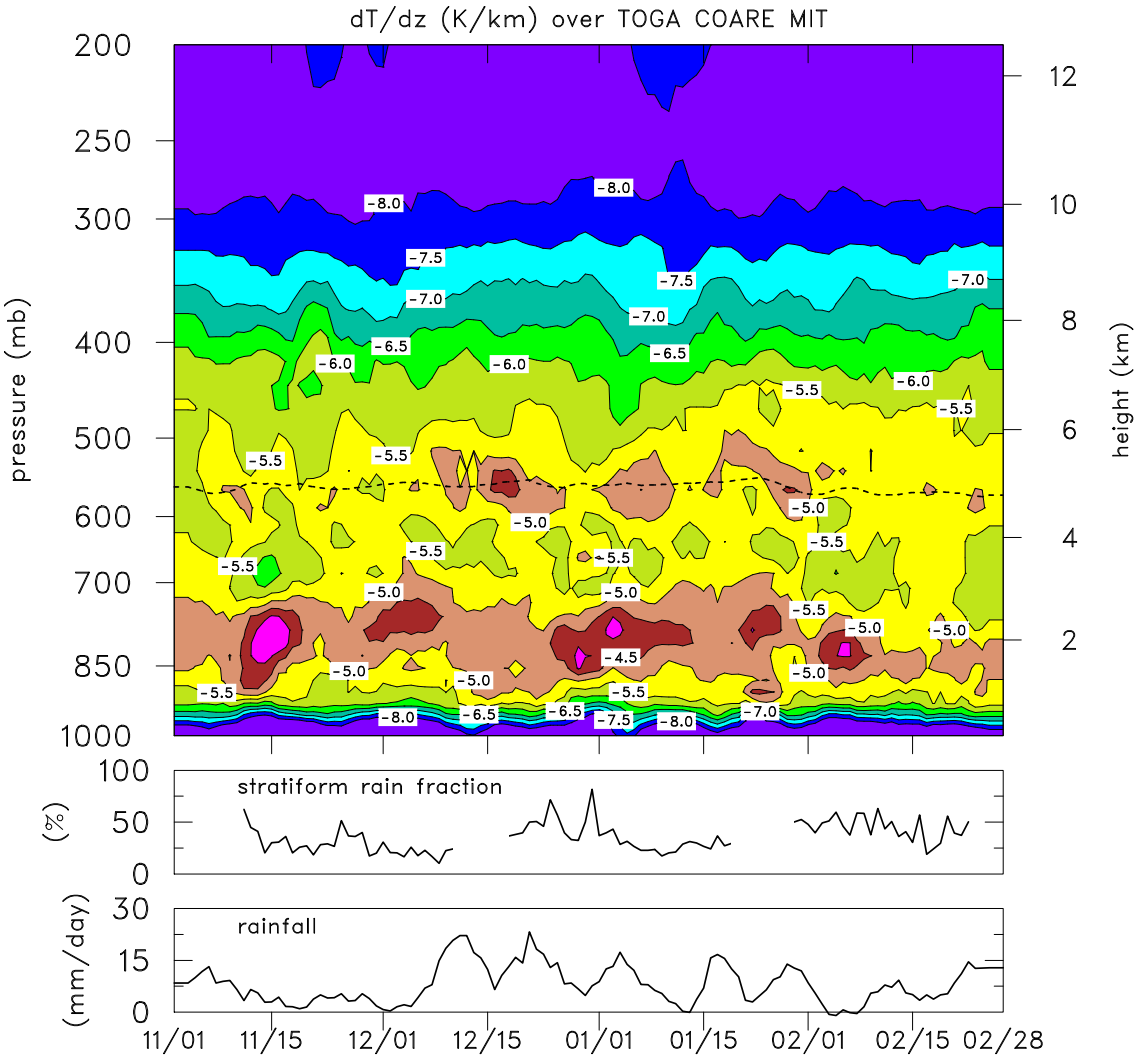


FIG. 8. (top panel) TOGA COARE IOP time series of static stability $dT/dz$, horizontal line indicates 0° level; (middle panel) time series of stratiform rain fraction; and (bottom panel) moisture-budget-derived rainfall. All fields are for MIT radar area.

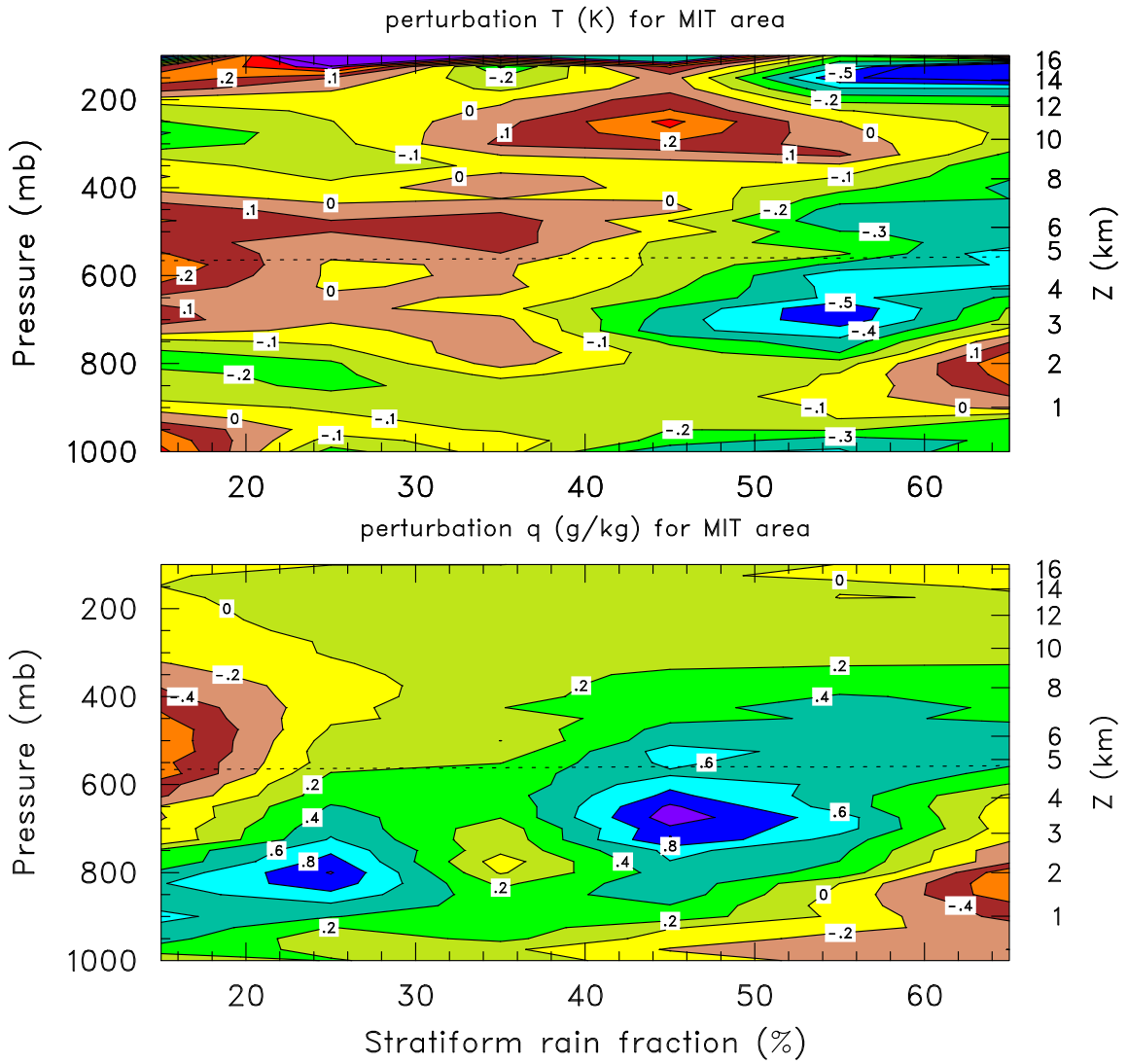


FIG. 9. Perturbation temperature (K; deviation from IOP-mean) and (bottom) perturbation water vapor mixing ratio (g kg$^{-1}$) as a function of stratiform rain fraction for the MIT radar coverage area during TOGA COARE for times when moisture-budget-derived rainfall over that area exceeded 3.5 mm day$^{-1}$. Dashed line indicates 0°C level.

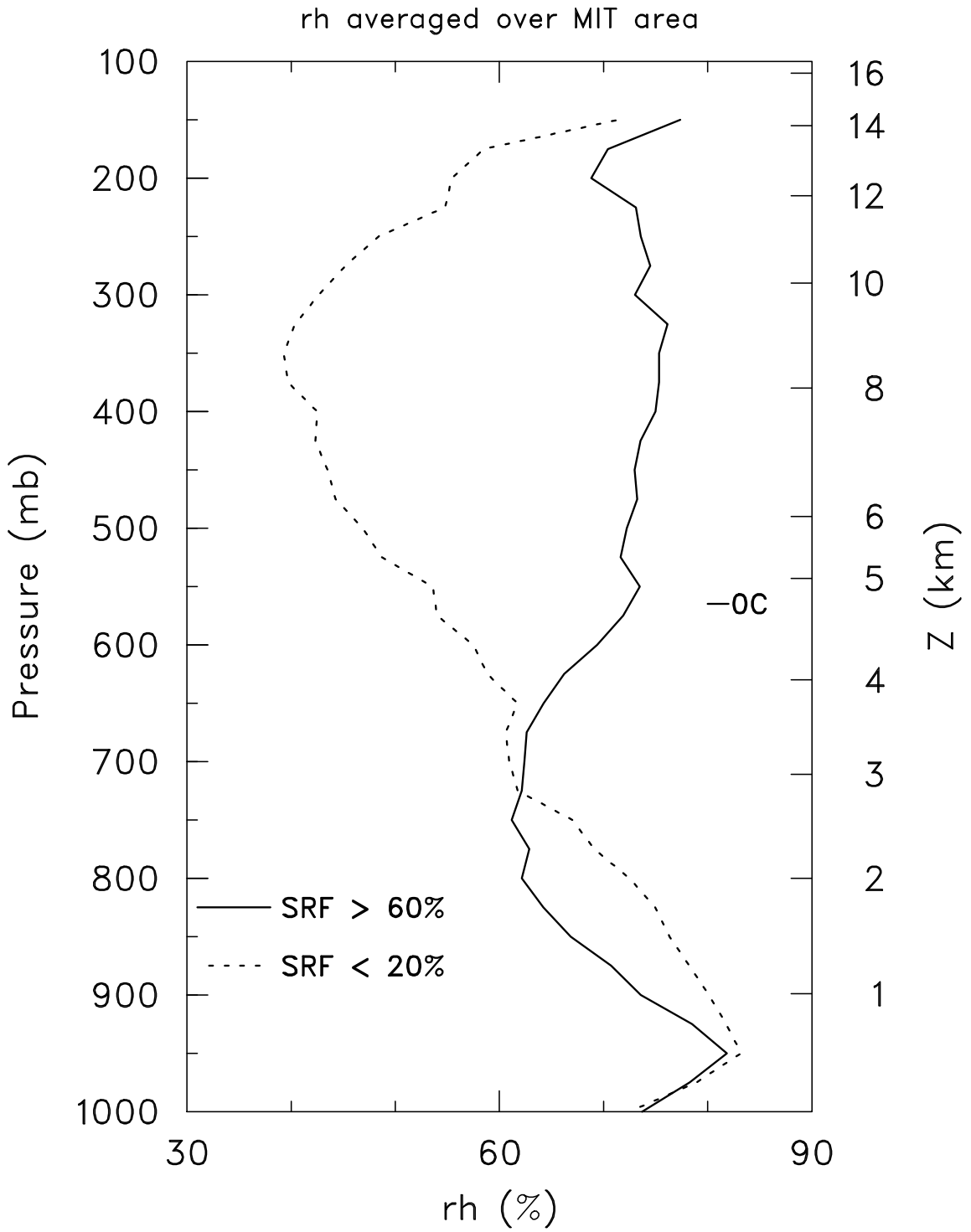


FIG. 10. Relative humidity (with respect to ice for $T < 0°C$) for stratiform rain fraction >60% (solid curve) and <20% (dashed curve).

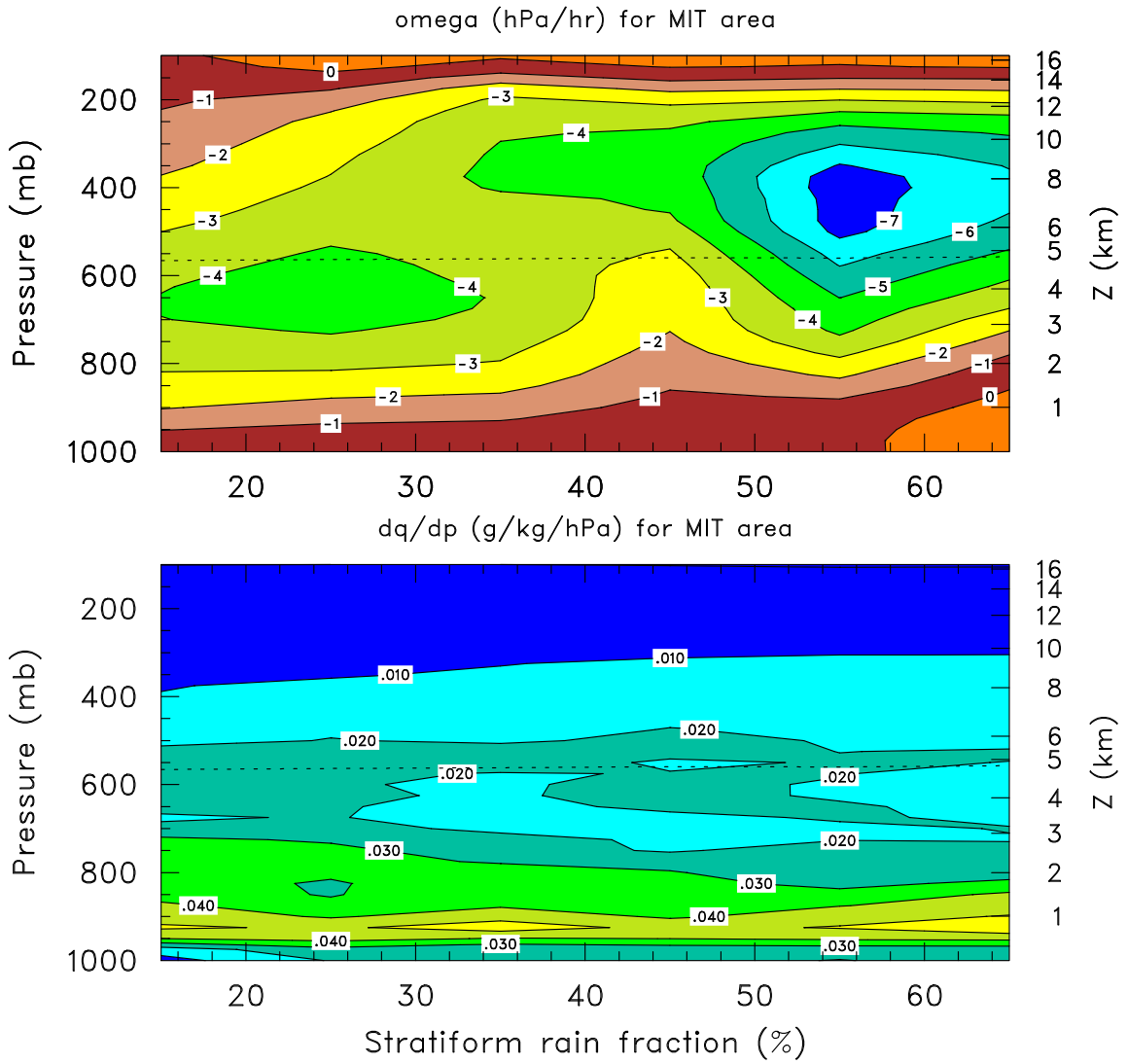


FIG. 11. (top) $\bar{\omega}$ (hPa h$^{-1}$) and (bottom) $dq/dp$ (g kg$^{-1}$ hPa$^{-1}$ as a function of stratiform rain fraction for the MIT radar coverage area during TOGA COARE for times when moisture-budget-derived rainfall over that area exceeded 3.5 mm day$^{-1}$. Dashed line indicates 0°C level.

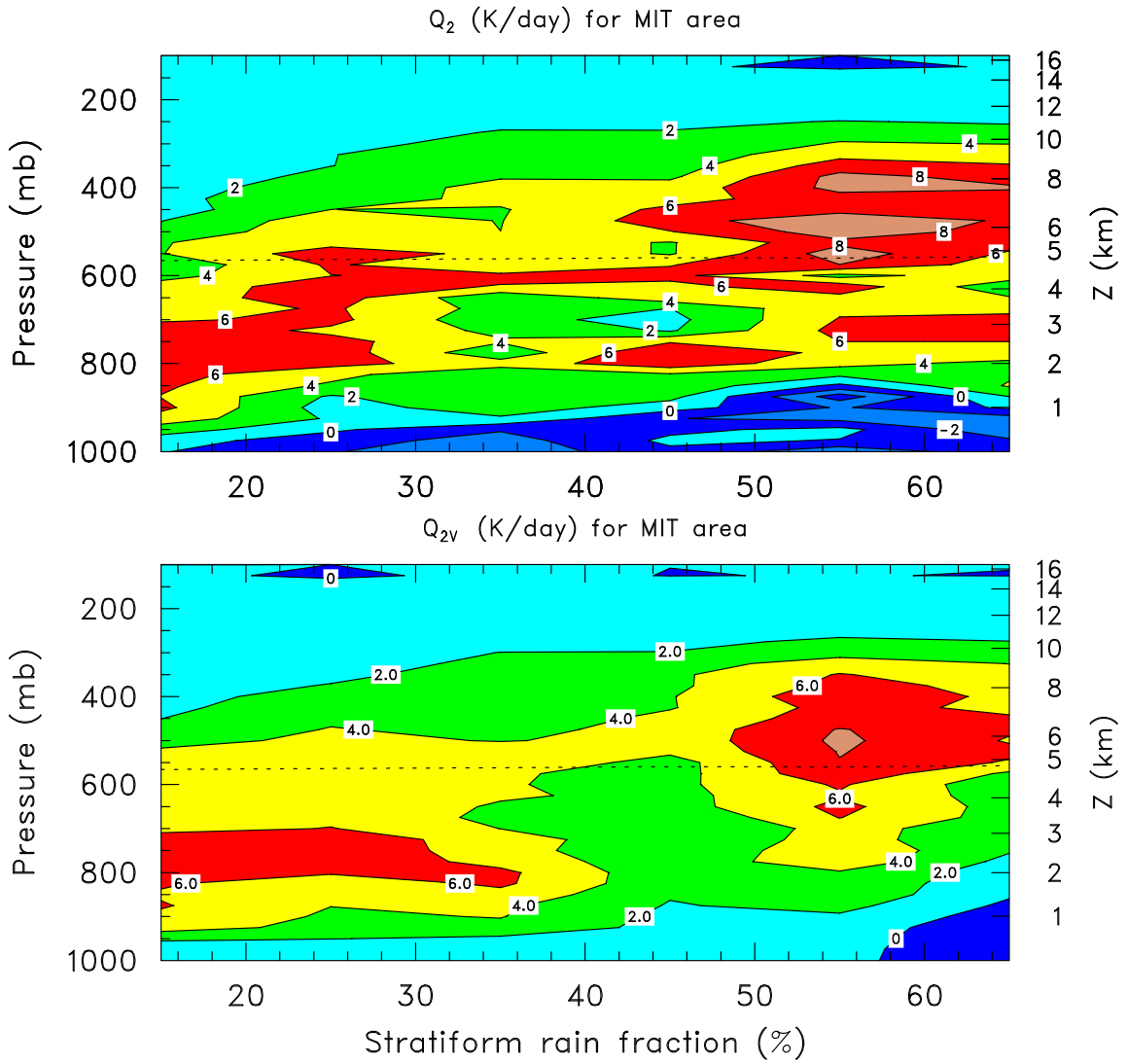


FIG. 12. (top) $Q_2$ and (bottom) $-L_v\bar{\omega}\partial\bar{q}/\partial p$ (K day$^{-1}$) as a function of stratiform rain fraction for the MIT radar coverage area during TOGA COARE for times when moisture-budget-derived rainfall over that area exceeded 3.5 mm day$^{-1}$. Dashed line indicates 0°C level.